

# Report on Northwestern's Air-Cooled, Copper Precipitation Hardened, High Strength, Weldable Steel Cast and Hot Rolled at Oregon Steel Mills

by  
Morris E. Fine  
Semyon Vaynman  
Gautam Ghosh  
September 27, 1996

---

## TABLE OF CONTENTS

- [Introduction](#)
- [Steel Composition and Mechanical Properties](#)
- [Welding of Steel](#)
- [Microstructure of NUCu-OSM Steel](#)
- [Estimate of Atmospheric Corrosion Resistance of NUCu-OSM Steel](#)
- [Summary](#)
- [Acknowledgment](#)
- [References](#)
- [Appendix 1.](#) Monotonic Tensile Stress-Strain Curves for NUCu-OSM Steel
- [Appendix 2.](#) Steel Compositions and Concentration Ranges in Data Bases Used for Atmospheric Corrosion Rate Estimates
- [Appendix 3.](#) Corrosion Indices and Equations
- Miscellaneous: [subject index terms](#) and [author contact information](#)

---

ITI technical report no. \_\_\_\_

---

### Introduction

During the past several years an easily weldable, high strength (more than 75 ksi yield), high impact fracture toughness steel (NUCu steel) has been investigated at Northwestern University with bridge applications in mind. For good weldability without pre-heating and post-heating, the carbon content of the steel was kept low and high strength was achieved by copper precipitation hardening. The steel was designed to be air cooled from low temperature hot rolling. Omitting the alloying elements (Cr and Mo), and the quench and temper heat treatment used in other high strength structural steel alloys reduces the cost of the steel, an important requirement for infrastructure applications. Also, chromium is undesirable in steel to be welded because of Cr<sup>+6</sup> formation. The steel is a variation of the Navy HSLA 80 and ASTM A710 steels which are usually quenched and tempered. In the NUCu steel 78 Ksi yield was reached in a plate up to 1 inch-thick plate without quenching or aging and the Charpy impact fracture toughness was very high.

The initial studies at Northwestern University were conducted on six 100-lb laboratory heats prepared at Inland Steel Company's Research Laboratory by vacuum-induction melting (1). These steel heats were hot-rolled to 1/2-inch-thick plates and air cooled. Mechanical properties and microstructure of these heats were investigated. Based on these results Oregon Steel Mills volunteered to produce a large commercial heat.

## Steel Composition and Mechanical Properties

A commercial 80 ton steel heat was produced at Oregon Steel Mills (OSM), Portland, Oregon. This report gives the results of our investigation of this steel, NUCu-OSM. The OSM heat was calcium treated for inclusion shape control. The analyzed composition of the steel produced by Oregon Steel Mills (NUCu-OSM) is listed in [TABLE 1](#). As mentioned before, the carbon content in the steel was kept low to improve weldability. Since the steel is not quenched and tempered, Cr and Mo were omitted as mentioned above. Copper concentration was approximately 1.35% to provide greater than 70 Ksi strength through precipitation hardening on air cooling. Ni was added to prevent hot-shortness during hot rolling. Nb and Ti were added to control grain size during hot rolling and welding.

Two slabs (6-inch-thick and 7-inch-thick) were cast using the Amsted bottom pressure casting process. The master slab was sectioned into smaller "child" slabs having dimensions as required for the finished plate size. Slab reheating was done by OSM in an auxiliary furnace maintained at the aim temperature of 1085°C with the range of 1075-1100°C. Soak time was 3 hours. Plates were reduced to final thicknesses, 1/2 to 1 inch, in a 4-high reversing mill and air cooled. Dropout temperature, temperatures at twice the final thickness (2T) and temperature of plates at final thickness recorded at OSM are summarized in [TABLE 2](#). The plates were hot rolled to final thickness without interruption. However, the 3/4-inch thick plate cobbled during hot rolling at 3-inch thickness. To save steel, this plate was re-heated and rolling continued.

Flat 1/4-inch-thick tensile specimens with a gauge section of 2 inches (ASTM E8 Standard) were machined from the middle thickness of the plates along the rolling direction. Standard size Charpy V-notch specimens (ASTM E23 Standard), machined from the middle thickness of the plate in the transverse orientation, were tested over -80 to +75°F temperature range.

The mechanical properties determined from the monotonic stress-strain curves of the steel plates produced at Oregon Steel Mills are summarized in [TABLE 3](#). Sample stress-strain curves are given in the Appendix. It is evident that steel has good ductility and the upper yield strength equals or exceeds 78 Ksi for all thicknesses investigated. [FIGURE 1](#) shows the upper yield stress dependence on the plate thickness. It decreases from 90 Ksi to 78Ksi as the thickness increases from 1/2 to 1 inch. Since cooling rate depends on the thickness of the plate, it is evident that lower cooling rate leads to lower strength. [FIGURE 2](#) shows the yield/UTS ratio as a function of plate thickness; this ratio on average is 0.9 with 0.84 being the lowest value observed.

The Charpy impact fracture toughness values of the 1/2, 5/8 and 1-inch-thick plates were very good, exceeding 63 ft-lbs at 10°F. In several samples the Charpy impact fracture toughness exceeded 264 ft-lbs, the limit of the machine ([TABLE 4](#)). However, the impact fracture toughness of the 3/4-inch-thick plate was lower than that of other plates. Microstructural investigation, described later, showed that the microstructure in this plate is different from that of the other plates. This was attributed to plate overheating during steel plate reheating after cobbling. As [FIGURES 3A](#) and [3B](#) indicate, the impact fracture toughness of NUCu-OSM steel is reduced if the steel is overheated. Similar behavior was observed also in our prior studies of the Inland Steel Co. laboratory heats. However, the very high fracture toughness of the steel is easily restored by re-heating at lower temperatures and air cooling. For example, reheating the specimens

made from plate "B2" (5/8-inch-thick) and plate "C1" (3/4-inch-thick) at 950°C for 30 minutes and air cooling dramatically improved fracture toughness ([TABLE 5](#)), however, it also resulted in reduction of yield stress to approximately 70 Ksi.

Tests were performed to determine the optimum reheating temperature that gives the best combination of strength and fracture toughness. To do that, tensile and Charpy specimens were first heated at 1250°C for 30 minutes and air cooled. Then specimens were reheated for 30 minutes at temperatures ranging from 500 to 1250°C, air cooled and tested. Results are summarized in [FIGURES 3A](#) and [3B](#). As expected, reheating of the steel to different temperatures affects the fracture toughness as well as the strength. A better combination of strength and toughness was obtained by reheating to approximately 1050°C; room temperature impact fracture toughness exceeded 264 ft-lbs while the yield strength was more than 76 Ksi.

In summation, NUCu-OSM steel has excellent strength-ductility-fracture toughness values if the slab reheat temperature does not exceed 1150°C or if steel is re-heated at 950 to 1050°C after hot rolling and air cooled. The origin of the variation in fracture toughness with rolling or reheat temperature will be discussed later in this report.

### **Welding of Steel**

Plates 5/8-inch-thick were welded manually with JETWELD 100M1MR (MIL 10018) electrode and automatically using the submerged arc process with LINCOLNWELD LA100 wire and LINCOLNWELD 880M flux without preheat or postheat. With automatic submerged arc welding heat input was 1.4 kJ/mm (designated as "low"), 2.7 kJ/mm (designated as "medium") and 3.9 kJ/mm (designated as "high"). The welded plates were sectioned and microhardness was measured across the plate-heat affected zone (HAZ)-weldment regions. Standard Charpy V-notch specimens were machined from the middle of the welded plates. Through-thickness oriented notches were placed in the HAZs, however, since the HAZs were very narrow, the fracture surface included the base plate, HAZ and weld regions. Thus, the values for impact fracture toughness reflect the characteristics of all three regions.

The hardness of the HAZ was slightly lower than that of the base plate as demonstrated in [FIGURES 4A](#) and [4B](#) for plate automatically welded with "low" and "high" heat input. The plate-HAZ-weld region had excellent fracture toughness ([FIGURE 5](#)) even with "high" heat input; even at -40°F the Charpy values were high: 101 ft-lbs (manual), 136 ft-lbs (automatic "low" heat input) and 38 ft-lbs (automatic "high" heat input).

### **Microstructure of NUCu-OSM Steel**

Dilatometry in a fully computerized MMC Quenching Dilatometer was performed to determine the A3 and Ms temperatures. The samples were heated to 1000°C at 10°C/min, held for 15 minutes and quenched by He gas. [FIGURES 6A](#) and [6B](#) show the heating and cooling curves for NUCu-OSM 1-inch-thick plate steel. The A3 temperature of this alloy is about 835°C, however a large difference was noticed in the Ms temperature in two runs (595 and 650°C).

A variety of techniques were used to characterize the microstructures of the alloys. Both grain size measurements and characterization of ferrite transformation products were carried out by optical metallography. Conventional transmission electron microscopy

(CTEM) and analytical electron microscopy (AEM) techniques were employed to investigate the substructure of the alloys, and the structure and the composition of the precipitates.

The microstructure of the as-received plates essentially consists of fully recrystallized polygonal ferrite grains. [FIGURE 7](#) shows the as-received microstructure of NUCu-OSM steel 1-inch-thick plate. The presence of a few pearlite colonies may be noted (marked P). The as-received plates invariably displayed a banded microstructure, especially at lower thicknesses as shown in [FIGURE 8](#) for 1/2-inch-thick plate. The average ferrite grain size in the banded regions was smaller by more than a factor of two. The remnants of banding were found to persist even after heating to 950°C for 30 minutes followed by air cooling.

The nature of the ferrite transformation product is a strong function of austenitizing temperature and subsequent cooling rate. [FIGURES 9A, 9B, 9C](#) and [9D](#) show the effect of normalizing heat treatment (austenitizing followed by air-cooling) on the microstructure of 1-inch-thick NUCu-OSM steel plate. Up to an austenitizing temperature of 1050°C, the transformed ferrite grains were essentially polygonal ([FIGURE 9A](#) and [9B](#)). In the temperature range of 1050 to 1150°C, a mixture of polygonal and allotriomorphic ferrite grains were observed ([FIGURE 9C](#)), however, they were predominantly polygonal. A heat treatment in the range of 950-1150°C yielded a more uniform ferrite microstructure compared to that of the as-received, air-cooled from hot rolling, state. At a solutionizing temperature of 1250°C ([FIGURE 9D](#)) or above, the austenite grains grow rapidly due to the dissolution of NbC particles which otherwise provide very efficient grain-boundary pinning. Extraction replicas from lower-temperature annealed or as-cooled NUCu-OSM steel examined in TEM showed the presence of very fine NbC precipitates. The composition of the particles were confirmed by EDS X-ray microanalysis in the AEM while the crystal structure was confirmed by electron diffraction. The results of ferrite grain size measurements versus austenitizing temperature are summarized in [TABLE 6](#).

A consequence of excessive grain growth is the formation of Widmanstätten ferrite plates upon subsequent cooling. Parallel arrangement of a large number of Widmanstätten ferrite plates, all nucleated at the prior austenite grain boundary and grown towards grain interiors, may be noticed in [FIGURE 9D](#). Such parallel arrangement is believed to minimize the strain energy associated with the displacive component of the transformation and also give rise to the phenomena of "self-accommodation". Widmanstätten ferrite plates are believed to form under paraequilibrium condition and at relatively small driving force. The lengthening of these plates continues at a constant rate as long as soft-impingement (overlap of diffusion fields) does not occur. The formation of Widmanstätten plates is usually complete within a fraction of a second. As shown in [FIGURE 10](#), the fracture crack propagates in steel with poor fracture toughness by a cleavage mechanism. It is obvious that the Widmanstätten ferrite plates provide a relatively easy path for crack propagation, giving rise to poor fracture toughness when the austenitizing before air-cooling is done at 1250°C. The origin of this might be the crystallography of the Widmanstätten ferrite plates.

Optical microscopy of the as-received 3/4 inch-thick plate ([FIGURE 11A](#)), that had low impact fracture toughness, shows a mixture of predominantly equiaxed and Widmanstätten ferrite. This microstructure indicates that this plate, sometime during its processing, was heated to a temperature higher than that for plates with higher fracture

toughness. Reheating this plate at 950°C for 30 minutes leads to recrystallized equiaxed ferrite grains ([FIGURE 11B](#)) and to good impact fracture toughness as shown in [TABLE 5](#).

Thin foil examination of the as-received 5/8- and 3/4-inch-thick steel plates revealed the presence of very fine scale (<10nm) coherent copper precipitates. [FIGURE 12A](#) shows a bright field TEM micrograph of as-received 5/8-inch-thick steel plate. [FIGURE 12B](#) is a selected area diffraction pattern (SADP) under [110] zone axis and it displays only BCC diffraction spots showing that these copper precipitates have the BCC structure. Nano-scale spherical Cu-precipitates, some of which are marked with an arrow, may be noticed in [FIGURE 12A](#). [FIGURES 13A](#) and [13B](#) show dark field images of Cu-precipitates in the same plate. [FIGURES 14A](#) and [14B](#) show the bright field micrographs of as-received 3/4-inch-thick steel plate with nearly spherical Cu-precipitates. Cu-precipitates are seen in dislocation-free regions ([FIGURE 14A](#)) as well as in the vicinity of dislocations ([FIGURE 14B](#)). Visual comparison of [FIGURES 12A](#), [12B](#), [14A](#), and [14B](#) suggests that the Cu-precipitates in the 3/4-inch-thick steel plate are slightly larger than in the 5/8-inch-thick plate. The dark field TEM micrograph of Cu-precipitates in the 3/4-inch-thick steel plate, shown in [FIGURE 15A](#), exhibit fringes suggesting that these precipitates are heavily faulted. This is also supported by the presence of a number of weak diffraction spots in the [110] zone axis SADP as evident from [FIGURE 15B](#). A structure of Cu-precipitates other than BCC and FCC has also been observed very recently by means of high resolution electron microscopy.

In particular, a  $9R$  (ABCBCACAB) structure of the Cu-precipitates formed at the early stages of aging in Fe-Cu and Fe-Ni-Cu alloys has been proposed. Upon heat treating the 5/8-inch-thick steel plate at 1050°C for 30 minutes followed by air cooling, the Cu-precipitates are found to be smaller than in the as-received condition. This is shown in the dark field micrograph in [FIGURE 16A](#) and the corresponding [111] zone axis SADP is shown in [FIGURE 16B](#). Unlike in [FIGURE 15B](#), no diffraction spot other than that from a BCC phase may be noticed in [FIGURE 16B](#). [FIGURE 17](#) shows a bright field TEM micrograph of the 5/8-inch-thick steel plate heat treated at 1250°C for 30 minutes and air cooled. Presence of a large number of dislocations, associated with the formation of Widmanstatten ferrite plates, may be noticed. Also, there is hardly any evidence of Cu-precipitates after this heat treatment, however, they must be present because the yield stress is high.

The prior austenite grain boundaries in an overheated to 1250°C 1/2-inch-thick plate were examined in AEM to investigate the possibility of any copper segregation. [FIGURE 18](#) is the bright field TEM micrograph showing a prior austenite grain boundary. The absence of any kind of precipitate in the grain boundary may be noted. The relative intensity of copper in the X-ray spectra obtained from the grain boundary was found to be the same as that obtained from the grain interior. Thus, there is no evidence that copper segregates into grain boundaries leading to poor impact fracture toughness of NUCu steel. Thus, the decrease in impact fracture toughness on heating to 1250°C and air cooling is attributed to formation of Widmanstatten ferrite.

### **Estimate of Atmospheric Corrosion Resistance of NUCu-OSM Steel**

Since NUCu steel with its high copper content falls outside the range of ASTM Standard G101 "Standard Guide for Estimating the Atmospheric Corrosion Resistance of Low-Alloy Steels", this Standard cannot be used to estimate the weathering resistance of

NUCu-OSM steel. The G101 corrosion index is based on the work by R.A. Legault and H.P. Leckie (2) utilizing part of an extensive data base published by C.P. Larabee and S.K. Coburn (3). This data base does not contain steels with Cu concentrations more than 0.5% (3). R.A. Legault and H.P. Leckie used a linear equation to describe the effect of elements on corrosion of steels (2). A power-law relationship is the actual relationship between corrosion rate and concentration of elements. Ten steels with the highest corrosion loss were omitted from C.P. Larabee and S.K. Coburn data base by R.A. Legault and H.P. Leckie in their analysis. Also, to compensate for non-linearity, square terms for concentration of Cu and some other elements were introduced leading to an equation that displays an increase in corrosion when Cu concentration exceeds 0.25%. It is well known, that the effect of Cu on atmospheric corrosion resistance of steels is most beneficial at low Cu concentrations but the effect continues to higher concentrations as shown in [FIGURE 19A](#) (4). C.P. Larabee and S.K. Coburn, on whose experiments ASTM G101 is based also show the experimental effect of copper on atmospheric corrosion of steels to follow an exponential equation ([FIGURE 19B](#)). Thus, there is no experimental evidence that increase of Cu over 0.25% leads to a dramatic increase in corrosion loss as implied by the R.A. Legault and H.P. Leckie equations and ASTM G101 Standard.

To estimate the corrosion performance of NUCu steel, we derived two power-law relationships between corrosion loss in marine environment (Kure Beach, NC) and composition of the steels utilizing two data bases:

1. C.P. Larabee and S.K. Coburn, all 270 steels are used (composition ranges are in appendix): (3)

$$\text{LOSS OF THICKNESS (MILS) 1N 15.5 YEARS} = 5.698(1.31\text{Cu} + 0.47\text{Ni} + 0.36\text{Cr} + 0.99\text{Si} + 1.33\text{P})^{-0.5552}$$

2. Data base from ASM Handbook of Metals (5), data collected by F.L. LaQue (4), 23 steels (composition ranges are in Appendix):

$$\text{LOSS OF THICKNESS (MILS) 1N 15.5 YEARS} = 34.849 (-48.3\text{C} + 10.0\text{Mn} + 28.5\text{Si} + 61.1\text{S} + 52.4\text{P} + 7.5\text{Ni} + 4.3\text{Cu} + 5.6\text{Cr} + 16.2\text{Mo})^{-0.644}$$

The Legault-Leckie equation for marine environment (Kure Beach, NC) has the following form (2) (C.P. Larabee and S.K. Coburn (3) data base. Data for 260 steels are used, ten steels are eliminated):

$$\text{LOSS OF THICKNESS (MILS) IN 15.5 YEARS} = 15.49 - 16.30\text{Cu} - 4.34\text{Ni} - 4.79\text{Cr} - 12.41\text{Si} - 32.01\text{P} + 2.93\text{CuNi} + 2.46\text{CuCr} + 4.36\text{CuSi} + 2.74\text{NiSi} + 12.82\text{NiP} + 1.75\text{SiP} + 16.60\text{Cu}^2 + 1.20\text{Cr}^2 + 4.25\text{Si}^2$$

[TABLE 7](#) compares the estimates of corrosion losses for typical A588, two steels (70W and 100W) that are being developed under the AISI/FHWA/US Navy High Performance Steels Initiative (compositions are in Appendix), and NUCu steel when Legault-Leckie and Northwestern University's equations are used. As expected, the Legault-Leckie equation grossly overestimates the corrosion loss by NUCu steel. The equations developed at Northwestern University demonstrate that corrosion resistances of all four steels are very close.

The corrosion losses for four steels, A242, A588, 0.21%Cu and 0.021%Cu, (compositions are in Appendix) estimated by the Legault-Leckie equation and the equations developed at Northwestern University are compared to experimentally determined losses (6) in [TABLE 8](#). This Table demonstrates that corrosion equation developed at Northwestern University give better estimates of corrosion losses for steels than Legault-Leckie equation.

[FIGURES 20A](#) and [20B](#) compare the experimental values for corrosion losses for 23 steels from LaQue data base (4) with predicted corrosion losses using Legault-Leckie equation and NU equations 1 and 2. It is obvious, that while predictions are good using the NU equations, corrosion loss predictions using the Legault-Leckie equation are poor especially at low and high measured corrosion rates.

As our analysis has shown NUCu steel should clearly be classified as a weatherable steel.

### **Summary**

This research has shown that a Grade 70 construction steel of 1/2- to 1-inch plate thicknesses can be produced without a quench and temper or accelerated cooling from hot-rolling if the Cu content in the steel is sufficiently high. Coherent very fine bcc Cu precipitates form on air cooling providing strengthening to at least 70 Ksi. The yield strength decreases with plate thickness from 90 Ksi for 1/2- inch-thick plate to 78 Ksi for 1-inch-thick plate. Investigation of 2inch-thick plate is underway.

While the fracture toughness of the steel is excellent when the hot-rolling temperature does not exceed 1150°C, overheating to 1250°C causes degradation in fracture toughness. This is related to growth of austenite grains and formation of Widmanstatten ferrite plates. Normalizing at 950 to 1050°C restores the room-temperature impact fracture toughness to above 264 ft-lbs while maintaining the yield strength of 70 Ksi or above.

No brittle heat-affected zone was formed during manual or automatic submerged arc welding without pre-heating or post-heating even at very high heat input. The fracture toughnesses in the plate and in the heat-affected zone were excellent. While the Cu in the HAZ dissolves when the temperature exceeds the solvus, it reprecipitates on cooling. Thus there is little degradation or little change in hardness in the HAZ. Since the carbon content is low, there is no decrease in fracture toughness in the HAZ.

Estimated by equations developed at Northwestern University, atmospheric corrosion losses for NUCu steel are not higher than those for other weathering steel grades.

### **Acknowledgment**

The experimental laboratory heats of steel were produced by Inland Steel Research Laboratory, East Chicago, Indiana. Dr. S.P. Bhat aided in the design of these steels. The commercial heat of steel was produced by Oregon Steel Mills, Inc., Portland, Oregon. Welding was performed by D. Hogan at welding facility of BIRL, Industrial Research Laboratory, Northwestern University. Consultations with S. Manganello were very helpful.

## References

1. M.E. Fine, R. Ramanathan, S. Vaynman, S.P. Bhat, "Mechanical Properties and Microstructure of Weldable High Performance Low Carbon Steel Containing Copper", "International Symposium on Low-Carbon Steels for the 90's", ASM, 1991, pp. 511-514.
2. R.A. Legault and H.P. Leckie, "Effect of Alloy Composition on the Atmospheric Corrosion Behavior of Steels Based on Statistical Analysis of the Larrabee-Coburn Data Set", in "Corrosion in Natural Environments", ASTM STP 55S, American Society for Testing and Materials, 1974, pp. 334-347.
3. C.P. Larrabee and S.K. Coburn, "The Atmospheric Corrosion of Steels as Influenced by Changes in Chemical Composition" in "First International Congress on Corrosion", London, Butterworth, 1962, pp. 276-285.
4. F.L. LaQue, "Corrosion Testing", Proceedings ASTM, Vol. 51, 1951, pp. 495-582.
5. "ASM Handbook on Metals", Volume 17 "Corrosion", 9th Edition, p. 543 (original source: H.R. Copson, "Long-Time Atmospheric Corrosion Tests on Low Alloy Steels", Proceedings ASTM, Vol. 60, 1960, pp. 650-665.
6. C.R. Shastry, J.J. Friel, H.E. Townsend "Sixteen-Year Atmospheric Corrosion Performance Of Weathering Steels In Marine, Rural, And Industrial Environments", in "Degradation of Materials In The Atmosphere", ASTM STP 965, 1988, pp. 5-15.

## Appendix 1. Monotonic Tensile Stress-Strain Curves for NUCu-OSM Steel

- [FIGURES 20A](#) and [20B](#). Monotonic stress-strain curves for (a) 1/2-, (b) 5/8-, (c) 3/4 and (d) 1-inch-thick plates in as-received condition.
- [FIGURES 21A](#), [21B](#), [21C](#), and [21D](#). Monotonic stress-strain curves for (a) 1/2-, (b) 5/8-, (c) 3/4 and (d) 1-inch-thick plates in as-received condition.

## Appendix 2. Steel Compositions and Concentration Ranges in Databases used for Atmospheric Corrosion Rate Estimates

- [TABLE 9](#). Chemical composition (wt.%) of Different High Performance Steels
- [TABLE 10](#). Chemical Composition (wt.%) of Steels Used in C.R. Shastry, J.J. Friel, H.E. Townsend Study ([6](#))
- [TABLE 11](#). Element Limits in Data Base by C.P. Larrabee and S.K. Coburn ([3](#)) (270 steels)
- [TABLE 12](#). Element Limits in LaQue Data Base from "ASM Handbook on Metals" ([5](#)) (original reference 4) (23 Steels)

## Appendix 3. Corrosion Indices and Equations

**Legault-Leckie Corrosion Equation** for Marine Environment (Kure Beach, NC) ([2](#)) developed for C.P. Larrabee and S.K. Coburn data set. ([3](#))

"...ten of the 270 experimental steels were omitted from this statistical analysis either because the data reported was estimated at one or more sites or because the data reported for one or more sites clearly represented statistical outliers." ([2](#))

LEGAULT-LECKIE CORROSION RESISTANCE INDEX =  $16.30\text{Cu} + 4.34\text{Ni} + 4.79\text{Cr} + 12.41\text{Si} + 32.01\text{P} - 2.93\text{CuNi} - 2.46\text{CuCr} - 4.36\text{CuSi} - 2.74\text{NiSi} - 12.82\text{NiP} - 1.75\text{SiP} - 16.60\text{Cu}^2 - 1.20\text{Cr}^2 - 4.25\text{Si}^2$

LOSS OF THICKNESS (MILS) IN 15.5 YEARS = 15.49 - (CORROSION RESISTANCE INDEX)

---

**NU Corrosion Equation #1** for Marine Environment (Kure Beach, NC) derived for C.P. Larrabee and S.K. Coburn data set. (3) Corrosion data for all 270 steels are used.

NU CORROSION RESISTANCE INDEX #1 =  $1.3\text{ICu} + 0.47\text{Ni} + 0.36\text{Cr} + 0.99\text{Si} + 1.33\text{P}$

LOSS OF THICKNESS (MILS) IN 15.5 YEARS =  $5.698 (\text{NU CORROSION RESISTANCE INDEX \#1})^{-0.5552}$

---

**NU Corrosion Equation #2** for Marine Environment (Kure Beach, NC) derived for data base from "ASM Handbook on Metals" (5) (23 steels):

NU CORROSION RESISTANCE INDEX #2 =  $-48.3\text{C} + 10.0\text{Mn} + 28.5\text{Si} + 61.1\text{S} + 52.4\text{P} + 7.5\text{Ni} + 4.3\text{Cu} + 5.6\text{Cr} + 16.2\text{Mo}$

LOSS OF THICKNESS (MILS) IN 15.5 YEARS =  $34.849 (\text{NU CORROSION RESISTANCE INDEX \#2})^{-0.644}$

**Subject index terms:**

1. Steel

**Author contact information:**

1. [Morris Fine <m-fine@northwestern.edu>](mailto:m-fine@northwestern.edu)
2. [Semyon Vaynman <svaynman@northwestern.edu>](mailto:svaynman@northwestern.edu)
3. Gautam Ghosh

**FIGURE 1**

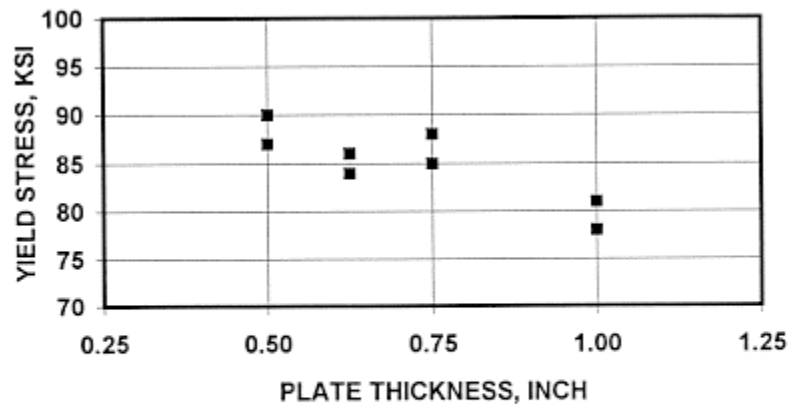


Figure 1. Effect of plate thickness on upper yield strength of NUCu-OSM steel air cooled after hot rolling.

**FIGURE 2**

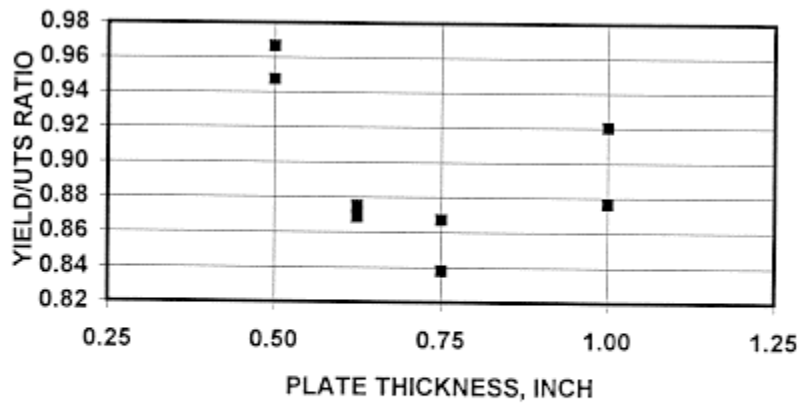
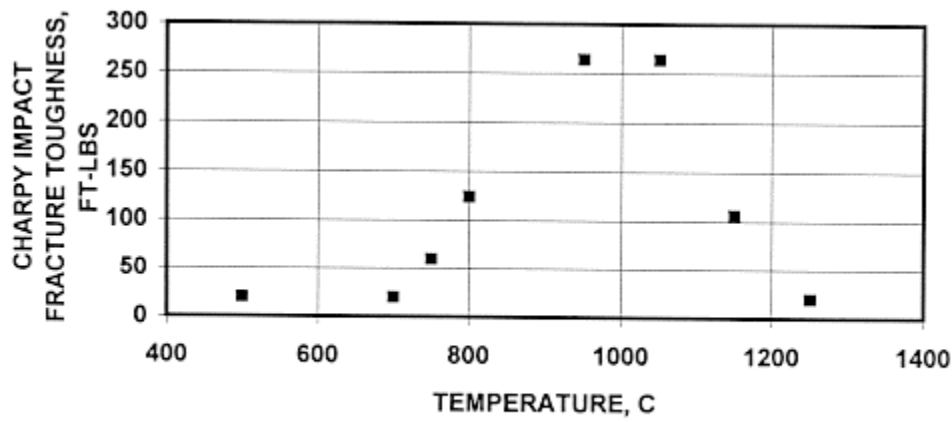


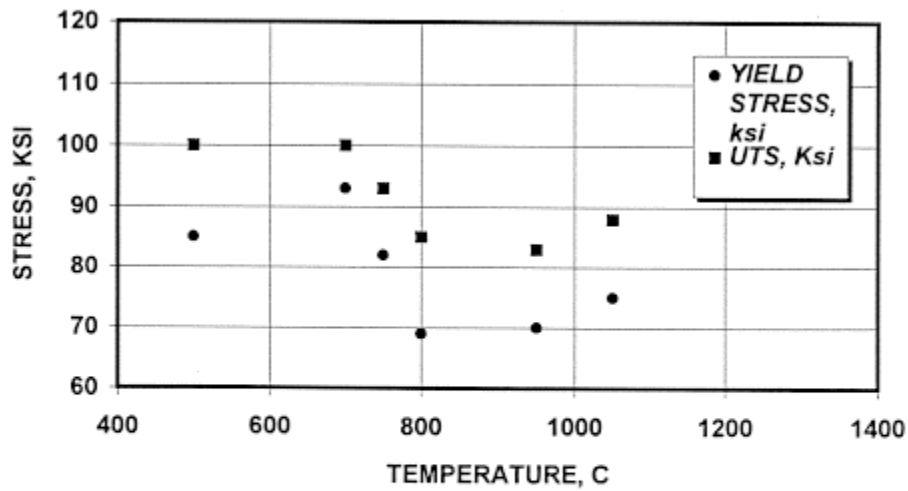
Figure 2. Yield/ultimate tensile strength ratio of NUCu-OSM steel air cooled after hot rolling for the different thicknesses plates.

**FIGURE 3A**



a

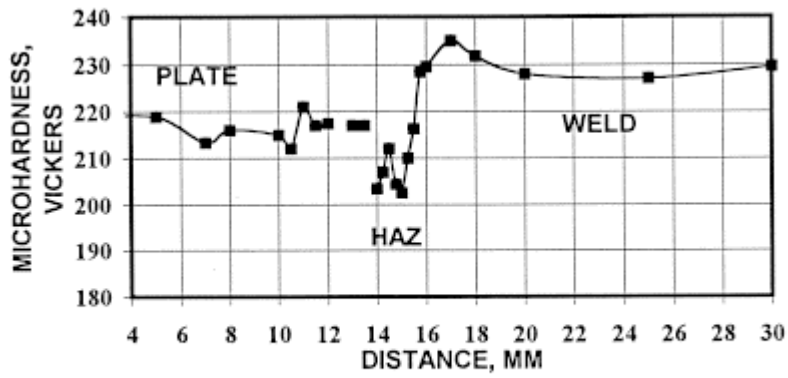
**FIGURE 3B**



b

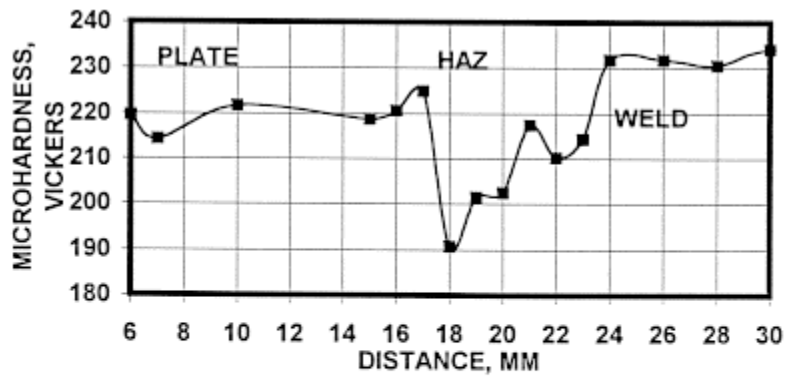
Figure 3. Effect of varying 30-minutes reheating temperature and air cooling on (a) impact fracture toughness and (b) yield and ultimate tensile stresses of NUCu-OSM steel at room temperature.

**FIGURE 4A**



a

**FIGURE 4B**



b

Figure 4. Microhardness profiles in NUCu-OSM steel-HAZ-weld regions. Welds were made by the automatic submerged arc process. Heat input:(a)1.4 kJ/mm - "low" heat input, (b)3.9 kJ/mm - "high" heat input).

**FIGURE 5**

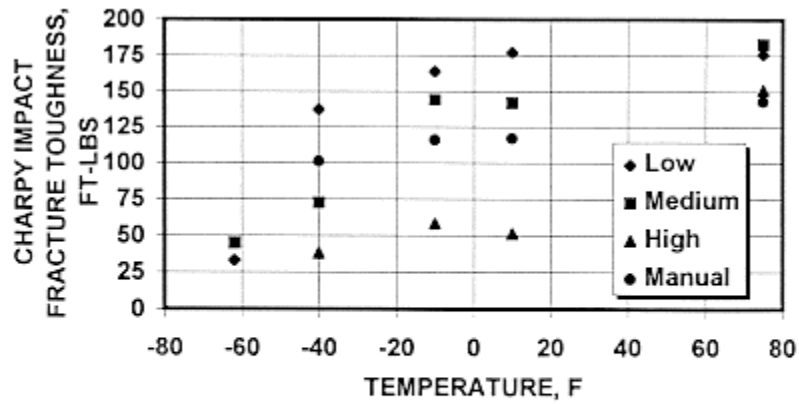
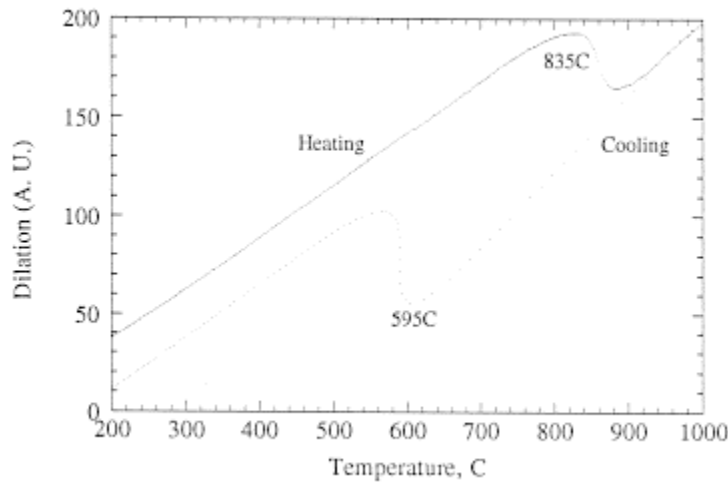


Figure 5. Charpy V-notch impact fracture toughness of plate-HAZ-weld regions in 5/8-inch-thick welded plates (1.4 kJ/mm - “low” heat input; 2.7 kJ/mm - “medium” heat input, and 3.9 kJ/mm - “high” heat input).

**FIGURE 6A**



## FIGURE 6B

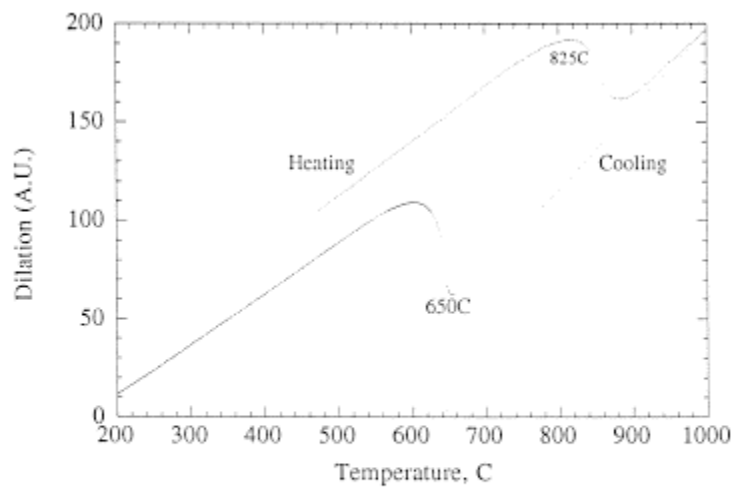


Figure 6. Dilatometry curves for 1-inch-thick NUCu-OSM steel plate (air cooled from hot rolling).

## FIGURE 7

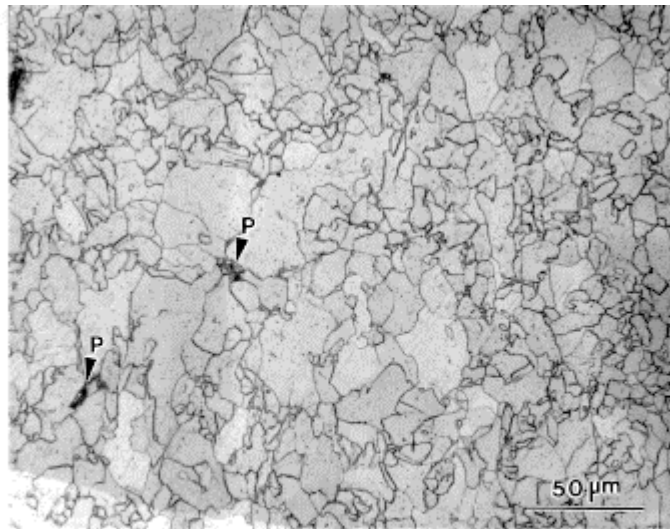


Figure 7. Optical micrograph of as-received (air cooled from hot rolling) 1-inch-thick NUCu-OSM steel. Sparsely distributed pearlite colonies are marked by P.

## FIGURE 8

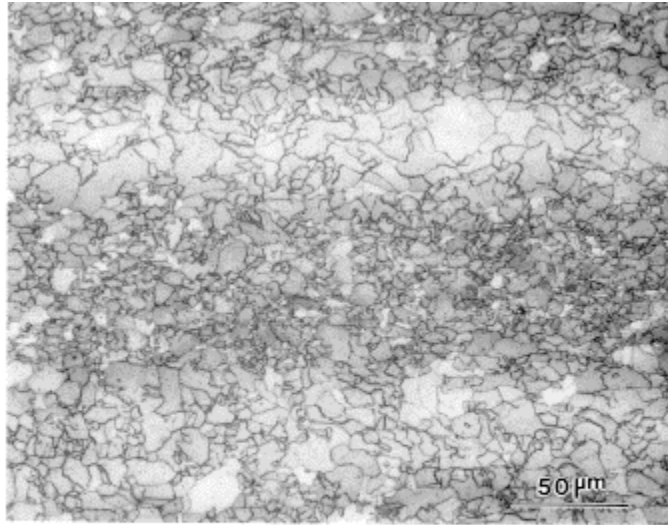
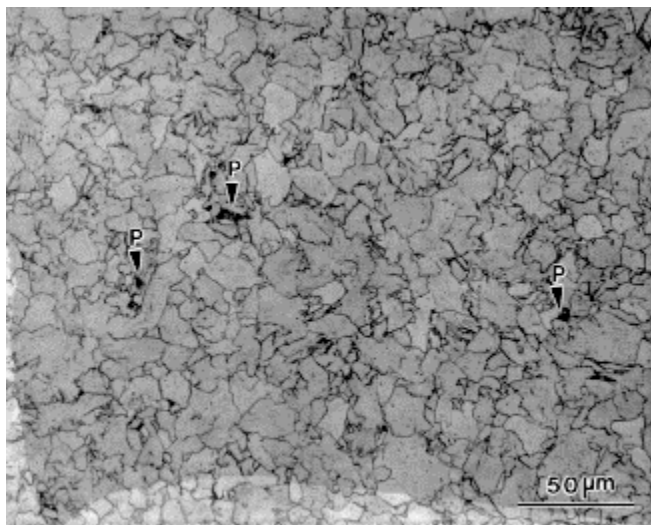


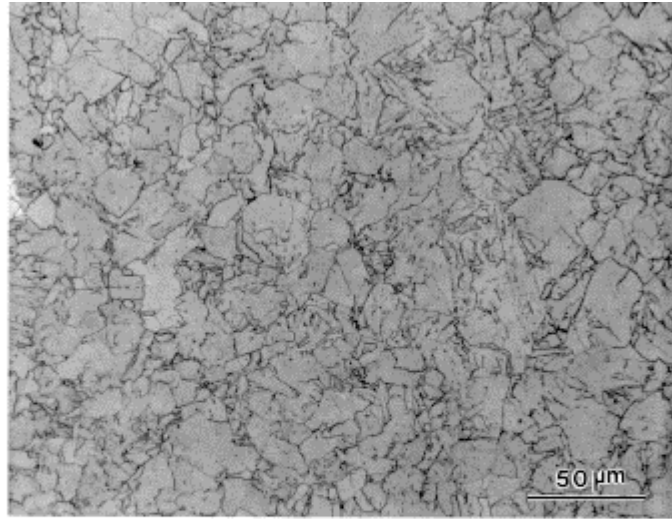
Figure 8. Optical micrograph of as-received (air cooled from hot rolling) 1/2-inch-thick NUCu-OSM steel showing heavily banded microstructure.

## FIGURE 9A



**a**

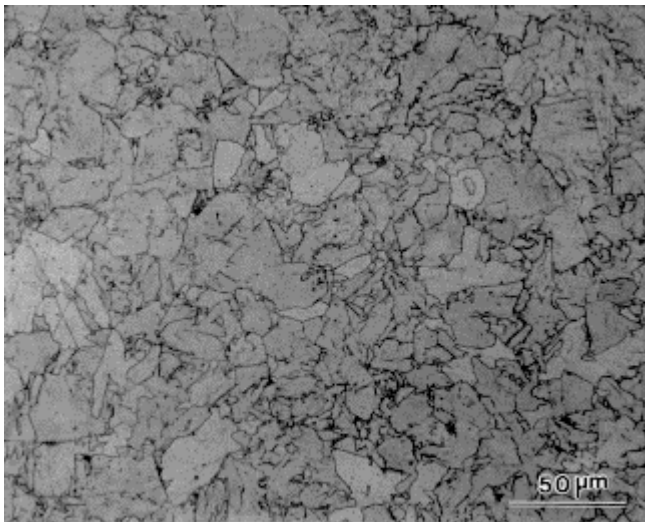
## FIGURE 9B



**b**

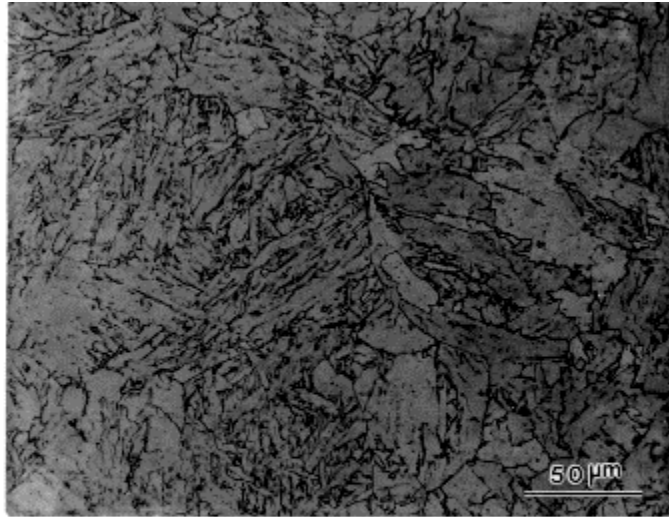
Figure 9. Optical micrograph of as-received 1-inch-thick NUCu-OSM steel showing the effect of heat treatment . In all cases they were solutionized for 30 minutes followed by air cooling: (a) 950°C, (b) 1050°C, (c) 1150°C, and (d) 1250°C.

## FIGURE 9C



**c**

## FIGURE 9D



d

Figure 9. Optical micrograph of as-received 1-inch-thick NUCu-OSM steel showing the effect of heat treatment . In all cases they were solutionized for 30 minutes followed by air cooling: (a) 950°C, (b) 1050°C, (c) 1150°C, and (d) 1250°C.

## FIGURE 10

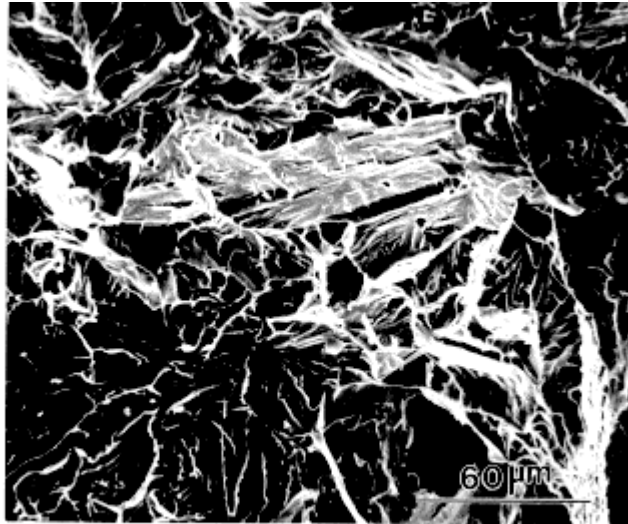
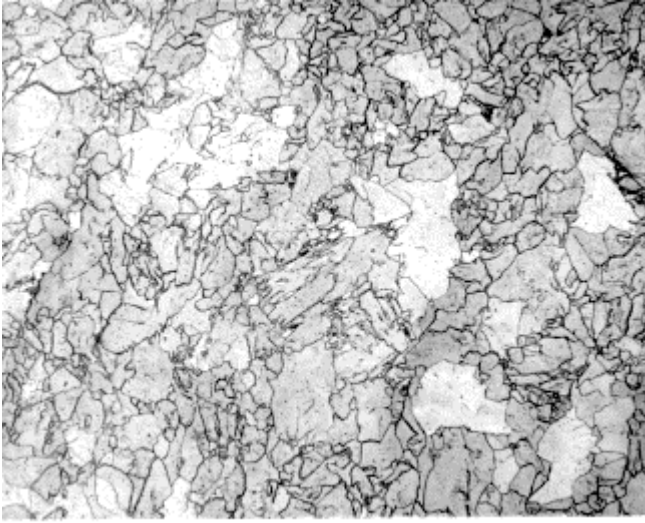


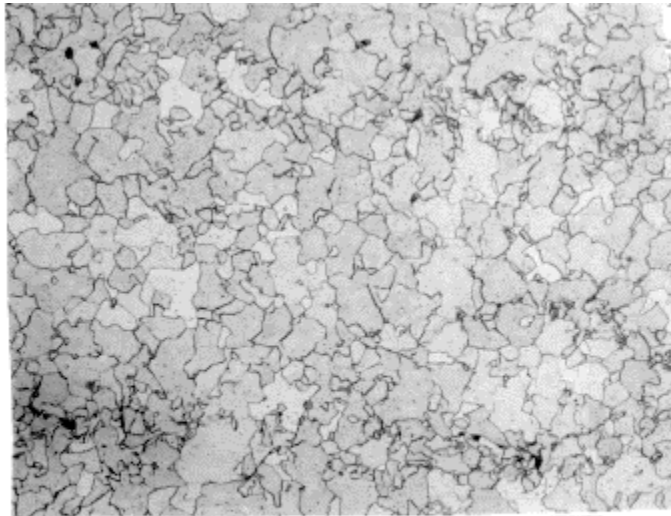
Figure 10. SEM fractograph of the overheated to 1250°C 1-inch-thick NUCu-OSM steel showing cleavage fracture.

**FIGURE 11A**



**a**

**FIGURE 11B**

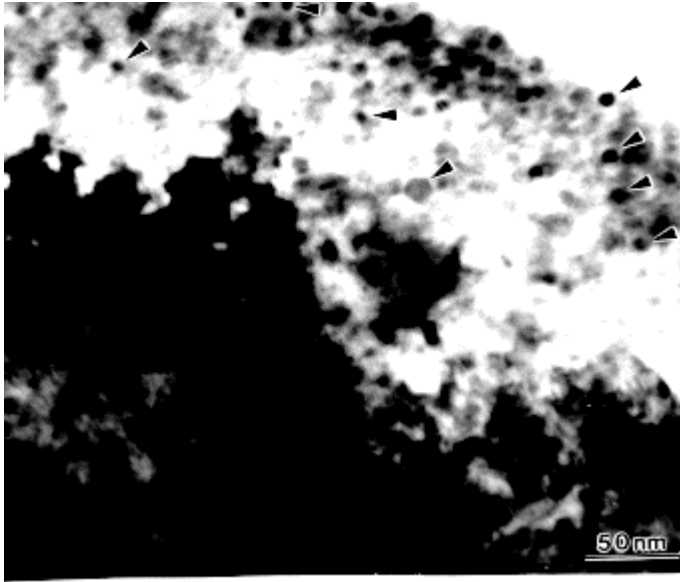


**b**

50 μm

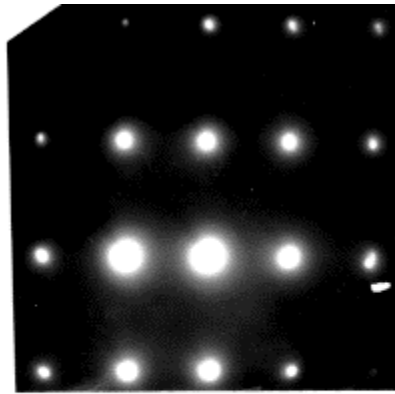
Figure 11. Optical micrograph of (a) as-received 3/4-inch-thick NUCu-OSM steel and (b) heated at 950°C for 30 minutes followed by air cooling

**FIGURE 12A**



**a**

**FIGURE 12B**



**b**

Figure 12. (a) Bright field TEM micrograph of as-received 5/8-inch-thick NUCu-OSM steel. Fully coherent nano-scale Cu-precipitates may be seen, some of which are marked with arrows, (b) selected area diffraction pattern under [110] zone axis.

**FIGURE 13A**

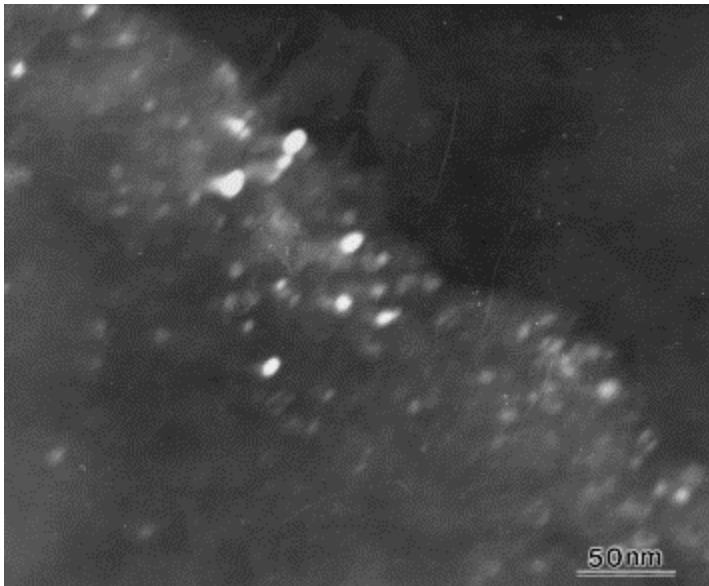


**FIGURE 13B**

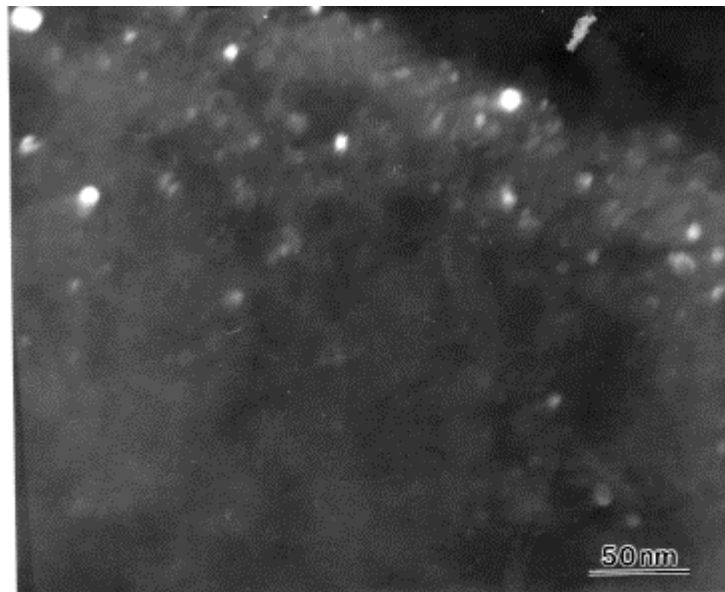
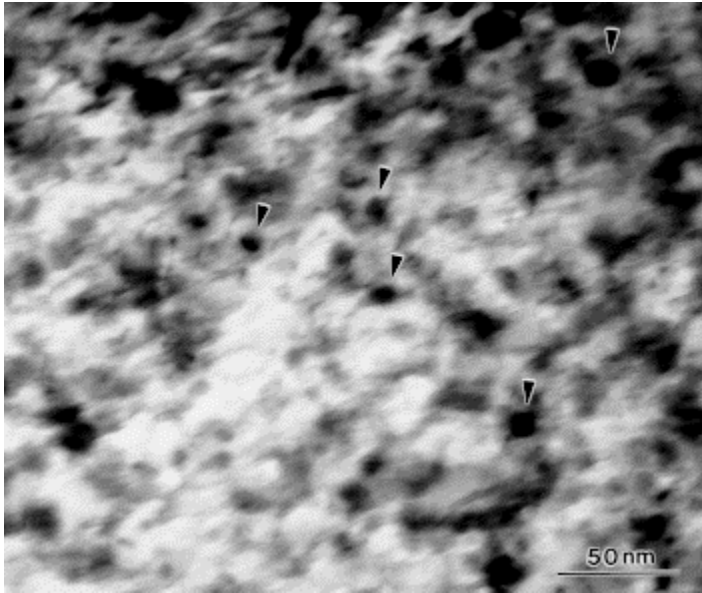


Figure 13. Dark field TEM micrographs of as-received 5/8-inch-thick NUCu-OSM steel showing nearly spherical Cu-precipitates.

**FIGURE 14A**



**FIGURE 14B**

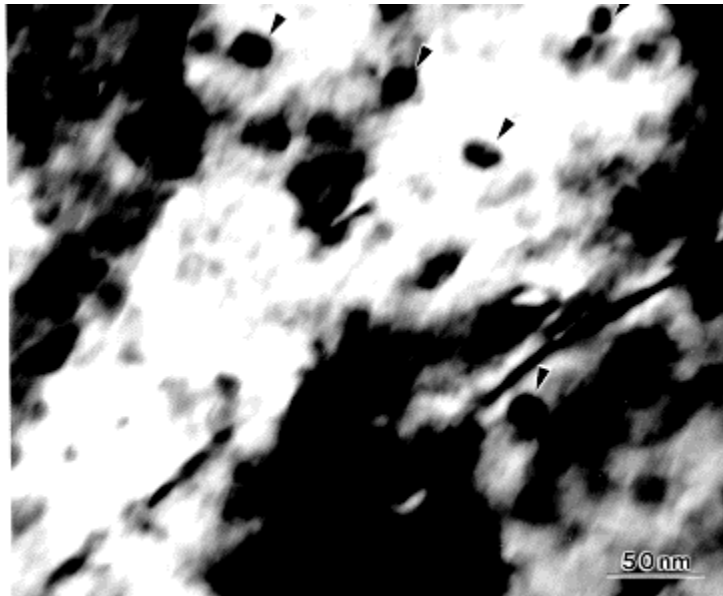
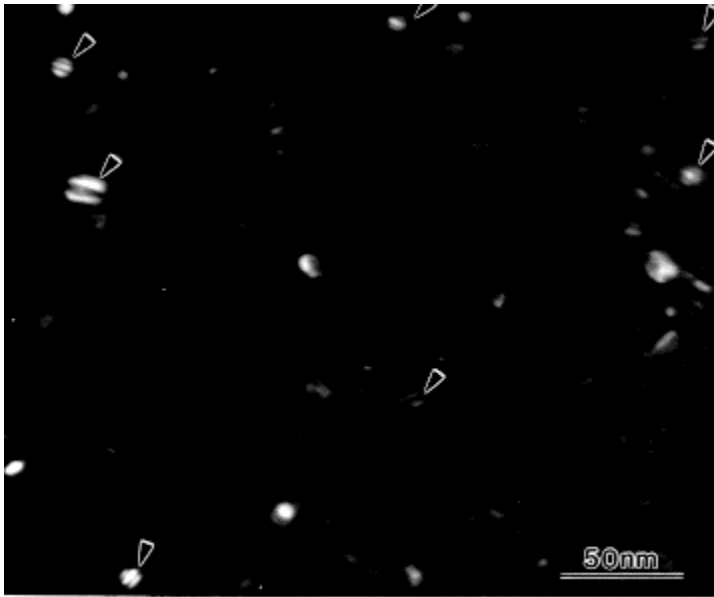


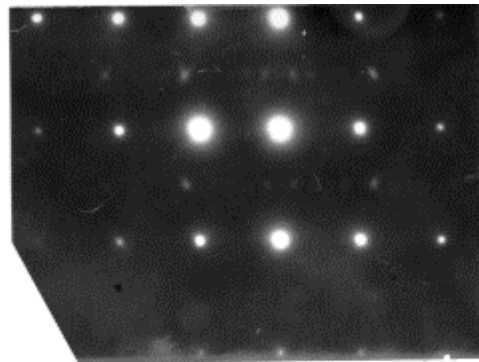
Figure 14. Bright field TEM micrograph of as-received 3/4-inch-thick NUCu-OSM steel showing sparsely distributed Cu-precipitates (marked with arrow).

**FIGURE 15A**



**a**

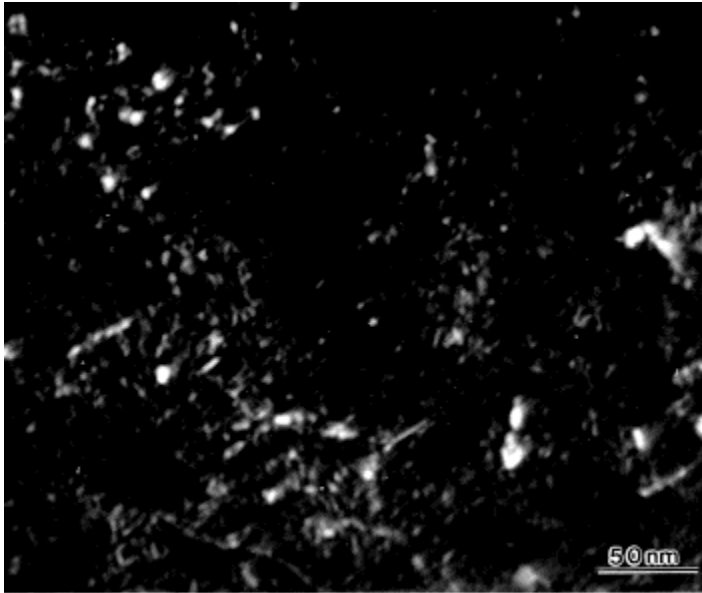
**FIGURE 15B**



**b**

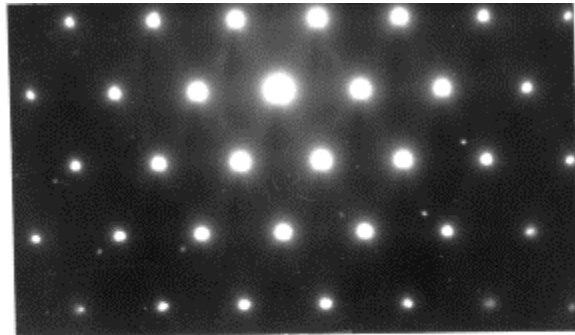
Figure 15. (a) Dark field TEM micrograph of as-received 3/4-inch-thick NUCu-OSM steel showing Cu-precipitates some of which are heavily faulted (marked with arrow), (b) selected area diffraction pattern under [110] zone axis.

**FIGURE 16A**



**a**

**FIGURE 16B**



**b**

Figure 16. (a) Dark field TEM micrograph of 3/4-inch-thick NUCu-OSM steel heat treated at 1050°C for 30 minutes followed by air cooling, (b) selected area diffraction pattern under [111] zone axis.

## FIGURE 17

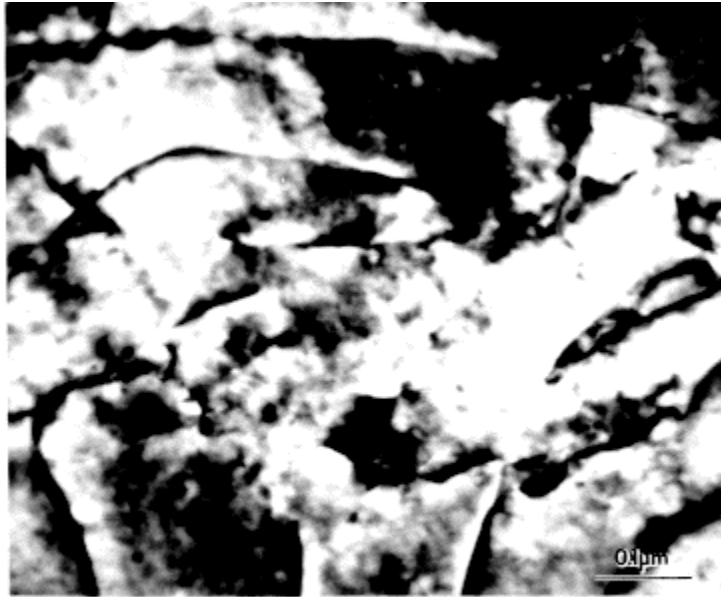


Figure 17. Bright field TEM micrograph of 5/8-inch-thick NUCu-OSM steel, heat treated at 1250°C for 30 minutes followed by air cooling, showing high density of dislocations associated with the formation of Widmanstatten ferrite plates.

## FIGURE 18

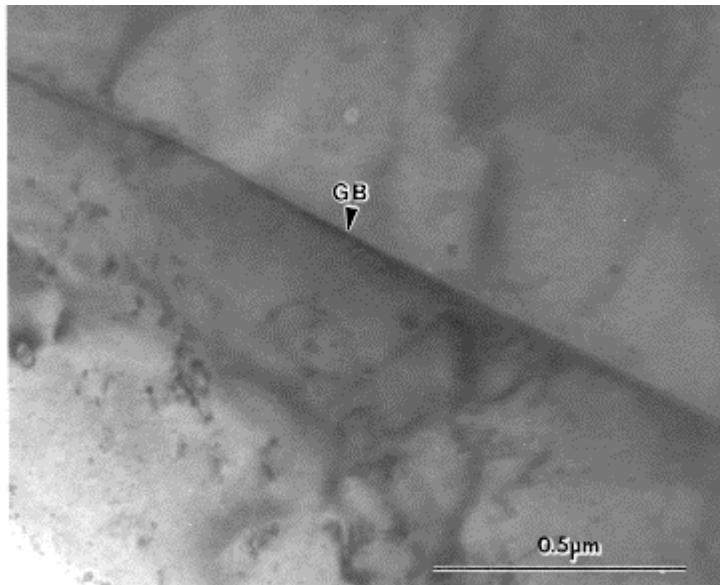
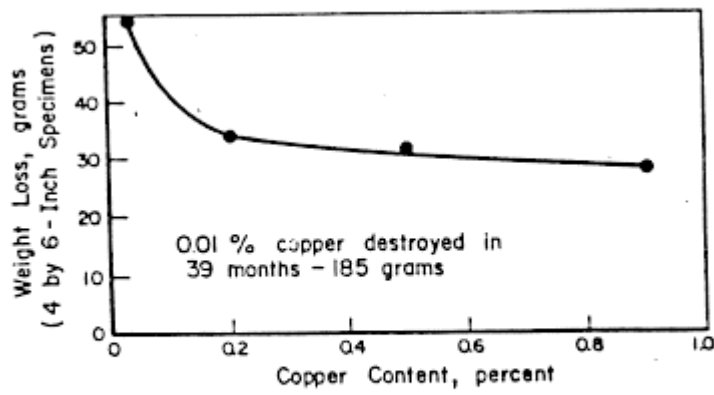


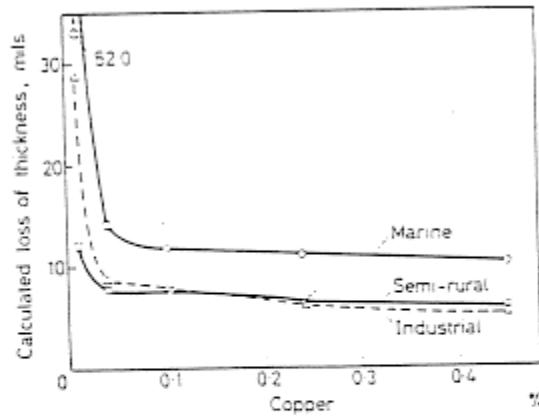
Figure 18. Bright field TEM micrograph of overheated to 1250°C 1/2-inch-thick NUCu-OSM steel showing the absence of any precipitate in the prior austenite grain boundary.

**FIGURE 19A**



**a**

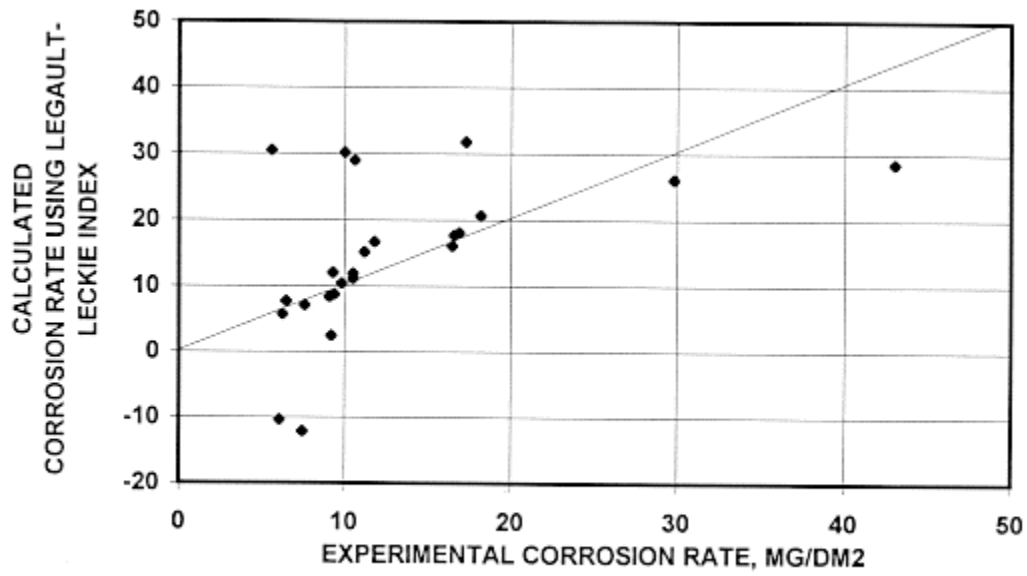
**FIGURE 19B**



**b**

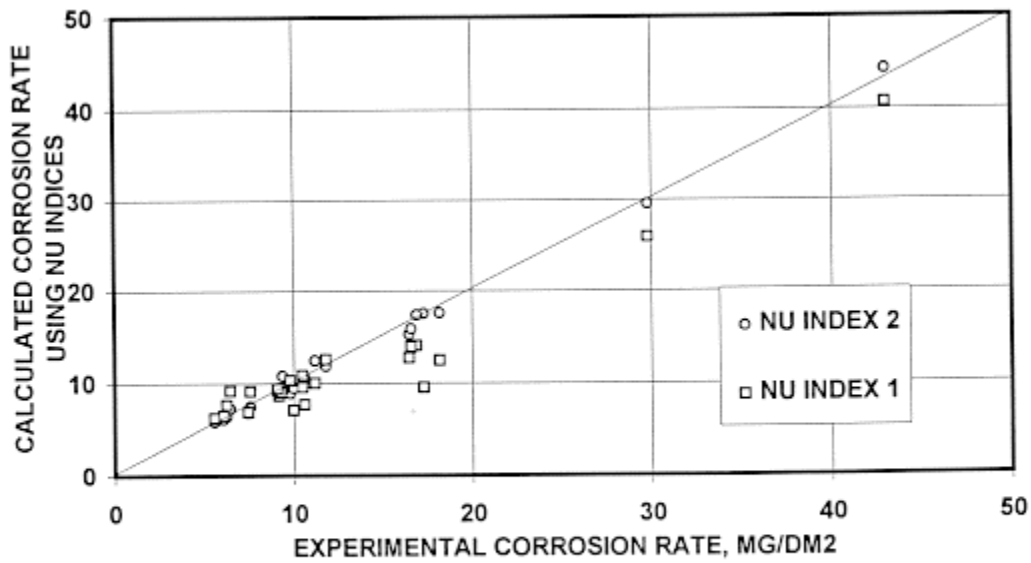
Figure 19. Effect of copper concentration on atmospheric corrosion of (a) Bessemer steel in marine environment (Kure Beach, NC)<sup>4</sup> and (b) steels from C.P. Larabee and S.K. Coburn data set<sup>3</sup> in different environments.

**FIGURE 20A**



a

**FIGURE 20B**



b

Figure 20. Experimental corrosion losses for 23 steels from LaQue data base<sup>4</sup> versus calculated corrosion losses using (a) Legault-Leckie and (b) NU equations.

**FIGURE 21A**

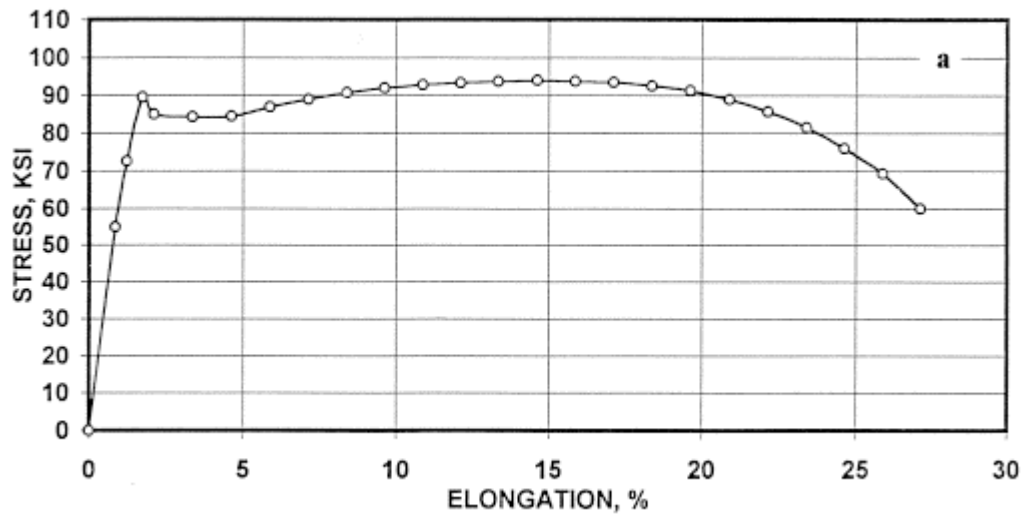


**FIGURE 21B**

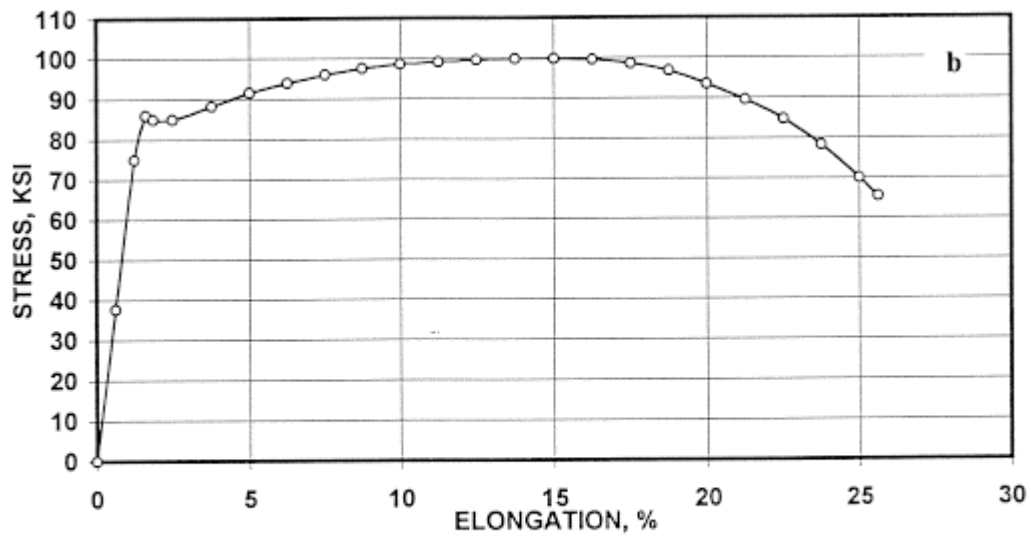
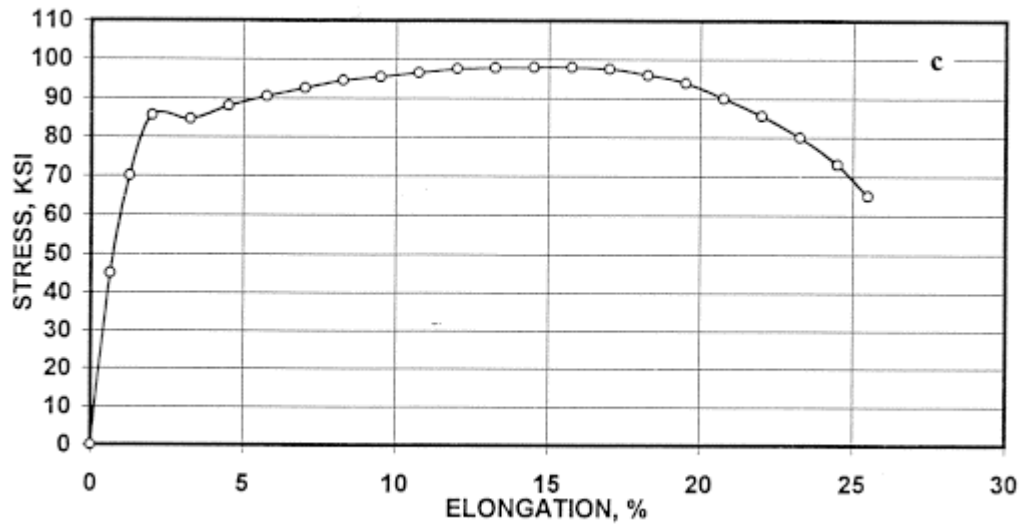


Figure 21. Monotonic stress-strain curves for (a)1/2-, (b)5/8-, (c)3/4 and (d)1-inch-thick plates in as-received condition.

**FIGURE 21C**



**FIGURE 21D**

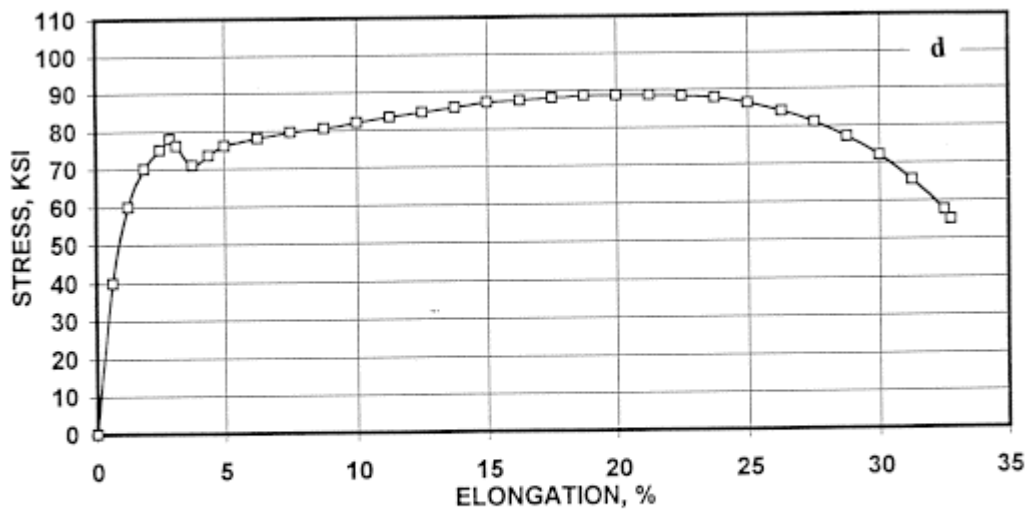


Figure 21. Monotonic stress-strain curves for (a)1/2-, (b)5/8-, (c)3/4 and (d)1-inch-thick plates in as-received condition.

## TABLE 1

Table 1. Composition of NUCu-OSM Steel (As Reported by OSM) (Wt.%)

ELEMENT	CONCENTRATION
C	0.03
Cu	1.35
Ni	0.84
Mn	0.49
Si	0.40
Nb	0.062
Ti	0.03

## TABLE 2

Table 2. Dropout and Rolling Temperatures for NUCu-OSM steel plates (As Reported by OSM)

FINAL PLATE THICKNESS, INCH	STEP NAME	THICKNESS, INCH	TEMPERATURE °C
1/2	Dropout	6	1090
	2T	1	890
	Final	1/2	840
5/8	Dropout	6	1090
	2T	1-3/8	900
	Final	5/8	830
3/4*	Dropout	6	1095
	2T	3*	910
	Final	3/4	830
1	Dropout	6	1080
	2T	2	940
	Final	1	800

\*Plate cobbled at 3 in. thickness. It was re-heated, straightened and the rolling continued.

**TABLE 3**

Table 3. Mechanical Properties of Hot Rolled and Air Cooled NUCu-OSM Steel

PLATE #	THICKNESS, INCH	$\sigma_{YIELD}$ , KSI	UTS, KSI	ELONGATION, %
A1	1/2	87	90	27
A2	1/2	90	95	28
B1	5/8	86	99	25
B2	5/8	84	96	26
C1	3/4	88	105	25
C2	3/4	85	98	26
D1	1	81	88	26
D2	1	78	89	32

**TABLE 4**

Table 4. Charpy Impact Fracture Toughness of Hot Rolled and Air Cooled NUCu-OSM Steel

PLATE No.	THICKNESS, INCH	IMPACT FRACTURE TOUGHNESS, FT-LBS AT TESTING TEMPERATURE, °F:					
		75	10	-10	-25	-40	-80
A1	1/2	222	180			162	132
A2	1/2	202	>264			193	142
B1	5/8	113	63			5	5
B2	5/8	145	126			10	5
C1	3/4	57	8				
C2	3/4	135	60	14	14		
D1	1	>264	>264			22	5
D2	1	>264		153	135	110	

**TABLE 5**

Table 5. Charpy Impact Fracture Toughness of NUCu-OSM Steel Normalized at 950°C for 30 Minutes

PLATE No.	IMPACT FRACTURE TOUGHNESS, FT-LBS AT TESTING TEMPERATURE, °F:					
	75	10	-10	-25	-40	-80
B2(5/8-inch-thick)	145		126			10
B2-N*	>264	>264	>264	174	>264	190
C1(3/4-inch-thick)	57		8			
C1-N*	>264		>264	>264	148	56

\* Specimens cut from plates B2 and C1 normalized at 950°C for 30 minutes and air cooled

## TABLE 6

Table 6. Grain size in NUCu-OSM 1-inch-thick plate in the as-received condition and after being heated to specified temperature for 30 minutes and air-cooled conditions.

TEMPERATURE, °C	GRAIN SIZE, $\mu\text{m}$ *
As received	7.49**
950	7.14**
1050	10.00**
1150	10.18**
1250	55.30***

\* mean linear intercept;

\*\* ferrite grain size;

\*\*\* prior austenite grain size

## TABLE 7

Table 7. Calculated Corrosion Losses for Few Steels in Marine Environment (Kure Beach, NC)

STEEL	CALCULATED CORROSION LOSS, MILS AFTER 15.5 YEARS USING:		
	LEGAULT-LECKIE CORROSION EQUATION (260 STEELS)	NU CORROSION EQUATION #1 (270 STEELS)	NU CORROSION EQUATION #2 FOR ASM DATA SET (23 STEELS)
A588	7.44	6.19	5.36
70W	5.80	5.16	4.10
100W	5.10	4.84	3.82
NUCu	22.34	3.37	4.12

The corrosion losses for four steels, A242, A588, 0.21%Cu and 0.021%Cu, (compositions are in Appendix) estimated by the Legault-Leckie equation and the equations developed at Northwestern University are compared to experimentally determined losses<sup>6</sup> in Table 8. This

## TABLE 8

Table 8. Calculated and Experimental Corrosion Losses for Four Steels Tested by C.R. Shastry, J.J. Friel, and H.E. Townsend<sup>6</sup> in Marine Environment (Kure Beach, NC)

STEEL	CALCULATED CORROSION LOSS, MILS AFTER 15.5 YEARS USING:			15.5 YEARS LOSS BASED ON EXPERIMENTAL DATA FROM REFERENCE (6)
	LEGAULT-LECKIE CORROSION EQUATION (260 STEELS)	NU CORROSION EQUATION #1 (270 STEELS)	NU CORROSION EQUATION #2 FOR ASM DATA SET (23 STEELS)	
A242	4.10	4.95	4.15	4.38*
A588	7.44	6.19	5.36	6.30*
0.21Cu STEEL	12.37	10.96	12.27	9.36*
0.021Cu STEEL	14.73	29.70	21.56	66.2*/**

\* Numerical data are calculated using equations describing effect of time (up to 16 years) on corrosion losses in these steels

\*\* Extrapolated value

## TABLE 9

Table 9. Chemical Composition (wt.%) of Different High Performance Steels

ELEMENT	CONCENTRATION (WT.%) IN STEELS			
	TYPICAL A588	HPS 70W*	HPS 100W*	NUCu-OSM
C	0.13	0.095	0.11	0.03
Mn	1.02	1.23	0.853	0.49
Si	0.22	0.40	0.299	0.40
S	0.018	low as pos.	0.003	0.005
P	0.008	0.012	0.015	0.005
Ni	0.27	0.32	0.850	0.84
Cu	0.21	0.33	0.329	1.35
Cr	0.64	0.55	0.540	0
Mo	0.20	0.06	0.458	0

\* Steels being developed under AISI/FHWA/US Navy High Performance Steels Initiative

## TABLE 10

Table 10. Chemical Composition (wt.%) of Steels Used in  
C.R. Shastry, J.J. Friel, H.E. Townsend Study<sup>6</sup>

ELEMENT	CONCENTRATION (WT.%)			
	A242	A588	0.21Cu STEEL	0.021Cu STEEL
C	0.09	0.13	0.02	0.07
Mn	0.65	1.02	0.35	0.35
Si	0.29	0.22	0.01	<0.001
S	0.032	0.018	0.013	0.025
P	0.11	0.008	0.005	0.009
Ni	0.66	0.27	0.02	0.01
Cu	0.27	0.21	0.21	0.021
Cr	0.52	0.64	0.02	0.02
V	....	0.062	....	....

## TABLE 11

Table 11. Element Limits in Data Base by C.P. Larrabee and S.K. Coburn<sup>3</sup> (270 steels)

ELEMENT	CONCENTRATION (WT.%)	
	LOWER LIMIT	UPPER LIMIT
Cu	0.008	0.49
Ni	<0.05	1.10
Cr	<0.10	1.30
Si	<0.10	0.64
P	<0.01	0.12

## TABLE 12

Table 12. Element Limits in LaQue Data Base from "ASM Handbook on Metals"<sup>5</sup> (original reference 4) (23 steels)

ELEMENT	CONCENTRATION (WT.%)	
	LOWER LIMIT	UPPER LIMIT
C	0.020	0.190
Mn	0.020	0.890
Si	0.002	1.000
S	0.010	0.050
P	0.005	0.140
Ni	0.004	4.990
Cu	0.030	1.090
Cr	0.000	1.190
Mo	0.000	0.240